ACS Infectious Diseases

Article

pubs.acs.org/journal/aidcbc

Cell-Based High-Throughput Screening Identifies Rifapentine as an Inhibitor of Amyloid and Biofilm Formation in *Escherichia coli*

Marie C. Maher, Ji Youn Lim, Cheston Gunawan, and Lynette Cegelski*

Department of Chemistry, Stanford University, Stanford, California 94305, United States

Supporting Information

ABSTRACT: *Escherichia coli* assemble functional amyloid fibers termed curli that contribute to bacterial adhesion, biofilm formation, and host pathogenesis. We developed a cell-based high-throughput screen to identify inhibitors of curli-mediated adhesion in the laboratory strain MC4100 and curli-associated biofilm formation in the uropathogenic *E. coli* clinical isolate UTI89. Inhibitors of biofilm formation can operate through many mechanisms, and such inhibitors could hold therapeutic value in preventing and treating urinary tract infections. The curli-specific screen allows the identification of compounds that inhibit either curli expression, curli biogenesis, or adhesion by normally produced curli. In screening the NIH Clinical Collection of 446 compounds, we identified rifapentine as a potent inhibitor in both of these screens. Rifapentine is an antibiotic used to treat tuberculosis that targets RNA polymerase, but prevents curli-dependent adhesion and biofilm formation in *E. coli* at concentrations below those that affect viability. Rifapentine inhibits curli production and prevents biofilm formation on plastic, on agar, and at the air−liquid interface by inhibiting curli gene transcription. Comparisons with a cephalosporin antibiotic further revealed that curli production is not affected by standard antibiotic treatment and cell killing pressure. Thus, we reveal a new role independent of killing activity for rifapentine as an inhibitor of curli and curli-mediated biofilm formation.

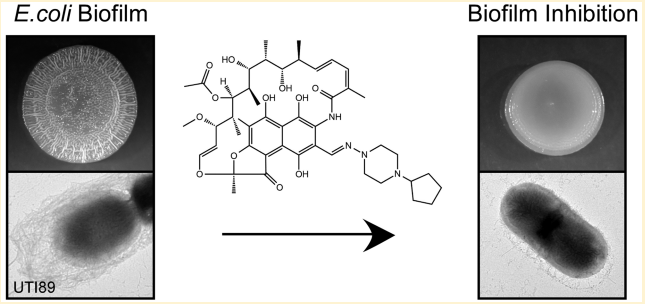

KEYWORDS: *uropathogenic E. coli, biofilm, adhesion, curli, functional amyloid, biofilm inhibitor*

Bacteria form multicellular communities termed biofilms that consist of the bacterial cells plus a self-produced extracellular matrix (ECM) that can contain various components including proteins, polysaccharides, nucleic acids, and lipids. Biofilms promote bacterial persistence as well as protection from environmental and chemical stresses.[1−4] In the human host, biofilms are associated with serious infectious diseases including cystic fibrosis pneumonia, infective endocarditis, recurrent urinary tract infection (UTI), periodontitis, chronic otitis media, and infections of medical devices such as intravenous catheters and artificial joints.[2,5,6] Biofilms can result in persistent infections that are difficult to treat, leading to further health complications and longer hospital stays. Several strategies have emerged to inhibit biofilm formation and eradicate established biofilms. These include preventing initial bacterial adhesion; interrupting quorum sensing mechanisms required for the gene expression of biofilm components; inhibiting the biosynthesis of the required protein or other extracellular components of the biofilm matrix; and identifying or tailoring enzymes that can degrade the biofilm matrix.[6,7]

A major challenge in targeting biofilm formation, particularly in preventing adhesion and the production and assembly of the extracellular matrix, is that different bacteria employ a diverse array of cell-surface adhesins and adhesive fibers as well as polysaccharides and matrix-building components.[6,8] At the same time, a given bacterial strain can also harbor redundant adhesive strategies such that a multipronged approach may be required to sufficiently disarm the bacterium.[7] Thus, detailed investigations are needed for each pathogen. Ultimately, such selective approaches for targeting specific biofilm formers are advantageous in potentially preventing a broad-spectrum influence across the host microbiome.

We have been examining adhesion and biofilm formation by uropathogenic *Escherichia coli* (UPEC), the major causative agents of urinary tract infections. UPEC employ an array of adhesive strategies in the host, presenting type 1 pili to adhere to bladder epithelial cells, P pili to adhere to kidney cells, and adhesive amyloid fibers termed curli that contribute to adhesion and biofilm formation.[9] Many important inhibitor efforts to date have focused on preventing type 1 pilus assembly (e.g., pilicides) and adhesion, given the role of the type 1 pilus as a bona fide virulence factor in UPEC bladder pathogenesis.[10,11] Yet, evidence has been emerging that curli also contribute to pathogenesis in vivo. Curli were identified in human patient urine samples by electron microscopy and by antibody reactivity, indicating that UPEC express curli within the human bladder,[12] and recent studies suggest that curli provide a fitness advantage to UPEC as reflected in bladder and kidney bacterial titers in the murine UTI model.[13] The host immune

Received: April 26, 2015
Published: July 27, 2015

DOI: 10.1021/acsinfecdis.5b00055
ACS Infect. Dis. 2015, 1, 460−468

response is also modulated depending on the expression of curli as well as cellulose,[12] and curli-expressing *E. coli* activate the production of pro-inflammatory cytokines (tumor necrosis factor-alpha, interleukin-6 and -8) in human sepsis and may contribute to inflammation during UTI.[14] Curli also contribute to the immune response by activating the Toll-like receptors (TLR1 and TLR2) and the CD14 complex.[15,16] Finally, a survey of clinical isolates from UTI in children found that the coexpression of curli and cellulose was most prevalent in isolates associated with severe UTI, particularly pyelonephritis.[17] Curli also have been ascribed roles in environmental persistence and transmission due to their ability to mediate adhesion to abiotic surfaces, such as stainless steel, and to biotic surfaces including plant leaves.[18−21] Adhesion to such substrates can contribute to foodborne outbreaks by pathogenic strains such as *E. coli* O157:H7.[22−24] In the laboratory, the coproduction of curli and cellulose enables the elaboration of bacterial biofilms formed on agar,[25] characterized by the hallmark wrinkled colony morphology, as well as biofilms at the air−liquid interface (pellicle) and biofilms attached to plastic (e.g., PVC).[26,27]

Curli are the most well-studied of the bacterial functional amyloids identified to date, yet amyloids have been identified as contributing to biofilm formation among *Salmonella* species,[30,31] *Bacillus subtilis*,[33] and numerous environmental biofilms.[26] In contrast to the amyloids associated with human disease that result from protein mis-assembly events, bacteria such as *E. coli* harness dedicated genetic and molecular machinery to assemble amyloid fibers at their cell surface for function.[28] Important aspects of curli biogenesis have been elucidated, yet more information is needed to fully understand the interactions and roles of protein machinery. Assembly of curli at the bacterial cell surface requires the coordination of several proteins encoded by the divergently transcribed *csgBA* and *csgDEFG* operons (*csg*, curli-specific genes).[28,29] In vivo polymerization of the major curli subunit, CsgA, into β-sheet-rich amyloid fibers depends on the nucleating activity of the minor subunit, CsgB.[30] CsgE, CsgF, and CsgG are assembly factors required for the stabilization and transport of CsgA and CsgB to the cell surface.[29,31] Thus, although the prevention of curli-associated biofilm formation may be of distinct value in interfering with pathogenesis in vivo, the identification of curli-specific assembly and adhesion inhibitors also provides value in a chemical genetics spirit to manipulate curli biogenesis and help to define the mechanisms of fiber assembly and adhesion.

The first small-molecule inhibitors of curli biogenesis, termed curlicides, were reported in 2008 and were discovered using low-throughput agar and broth-based assays.[32] These were ring-fused 2-pyridones identified among a set of compounds that were under study for their ability to prevent amyloid fiber formation of the β-amyloid protein associated with Alzheimer's disease. One compound, FN075, a dual curlicide and pilicide, was effective in decreasing bladder colonization by UPEC in the mouse cystitis model.[32]

In this work, we implemented two high-throughput screens designed to identify inhibitors of curli-mediated adhesion and curli-associated biofilm formation in UPEC. The screens rely on the detection of biomass accumulation in 384-well plates. The curli-specific screen employed the K12 laboratory strain MC4100[33] that produces curli only at the cell surface and does not produce cellulose. Reduced biomass accumulation can result from the inhibition of curli biogenesis (either through altered gene expression or aberrant fiber assembly) or by interrupting adhesive interactions between normally curliated cells and the assay well surface. A second screen employed the UPEC clinical isolate UTI89 that requires curli for biofilm formation in the given growth conditions, but also requires cellulose and potentially other factors.[32,34] Rifapentine was identified as a potent inhibitor in each of these screens using the NIH Clinical Collection small-molecule library. We discovered that rifapentine, at low micromolar and submicromolar concentrations, did not inhibit cell viability and prevented curli gene transcription and biofilm formation. Results with rifapentine are presented together with other rifamycin antibiotics as well as an unrelated antibiotic, Cefaclor, that does not influence curli production.

RESULTS AND DISCUSSION

Development of the Curli-Dependent Biofilm Inhibitor Screen. In designing a high-throughput screen (HTS) to identify inhibitors of curli-dependent UTI89 biofilm formation, we optimized bacterial growth parameters and the biomass detection method to measure the extent of biofilm formation in a 384-well plate format. In such a HTS format, one wants to minimize washes or reagent transfers to the maximum extent possible. The traditional crystal violet based biofilm formation assay in 96-well plate format[35] is not ideal for a higher throughput 384-well plate screen due to the many necessary liquid handling steps and its limited sensitivity. We sought an alternative assay and were successful in employing BacTiter-Glo as a biofilm detection method. BacTiter-Glo is a proprietary formulation that uses luciferase to generate luminescence from liberated ATP upon cell lysis and has been used to estimate relative cell numbers in other high-throughput screens. We note that an attractive assay design that was successful in a *Pseudomonas aeruginosa* HTS involving BacTiter-Glo detection and biofilm formation on polypropylene 384-pin lids[36] was not suitable for UTI89 biofilms and did not show a significant difference in cell adherence between UTI89 and the curli mutant, UTI89Δ*csgA* (data not shown). Indeed, assay parameters must be optimized for each organism of interest due to differences in the mechanisms of biofilm formation. We employed the more traditional biofilm assay based on adherence to well walls coupled with the luminescence-based detection of BacTiter-Glo.

PVC plates are commonly used for UTI89 and other *E. coli* biofilm assays in 96-well plate format, but are not available in 384-well plate format. Growth in PVC plates would also not be ideal because PVC plates cannot be used directly for optical detection of visible light or luminescence and would require a transfer of all well contents to a detection plate. Finally, clear-bottom plates would be preferable in allowing a simple determination of cell growth by measuring the optical density at 600 nm before wells are rinsed to subsequently quantify the adherent cells. Thus, we tested commercially available polystyrene plates with a variety of surface treatments to select an optimal plate type. In addition, although a growth time of ∼48 h is necessary to produce sufficient biomass accumulation for detection in the traditional CV assay, we examined whether the sensitivity of the BacTiter-Glo assay and biofilm formation in 384-well plate format could allow analysis at shorter growth times. Bacteria were grown in YESCA nutrient broth, which results in curli-dependent biofilm formation and curli-associated phenotypes. Untreated polystyrene plates were not suitable for assaying biofilm formation and yielded high luminescence values for both UTI89 and UTI89Δ*csgA* (Figure

DOI: 10.1021/acsinfecdis.5b00055
ACS Infect. Dis. 2015, 1, 460−468

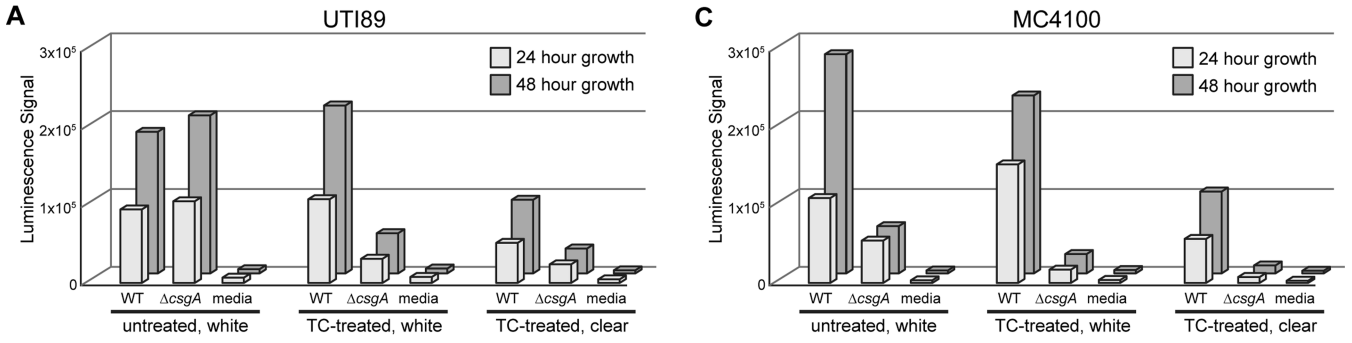

B

Relative Signal Intensity (WT strain vs. Mutant)

24 hr	0.90	3.47	2.18
48 hr	0.90	4.19	2.99

Z′ (WT vs. Media)

24 hr	0.80	0.63	0.62
48 hr	0.76	0.83	0.66

Z′ (WT vs. Mutant)

24 hr	-3.21	0.30	-0.23
48 hr	-5.61	0.50	0.05

D

Relative Signal Intensity (WT strain vs. Mutant)

24 hr	2.00	8.98	7.74
48 hr	4.64	9.25	10.61

Z′ (WT vs. Media)

24 hr	0.44	0.60	0.47
48 hr	0.64	0.69	0.26

Z′ (WT vs. Mutant)

24 hr	-1.29	0.52	0.32
48 hr	0.34	0.59	0.14

Figure 1. Comparison of UTI89 curli-associated biofilm formation as a function of plate type and growth time. (A) Comparative plots of BacTiter-Glo luminescence to quantify relative amounts of UTI89 (left) and MC4100 (right) biomass accumulation as a function of plate type and growth time. Each bar is the average luminescence measurement of 98 wells. Error bars are not shown for clarity, but are reflected in the Z' values. (B) Numerical list of relative luminescence intensities in the presence and absence of compound and associated Z' values from plates in which the edge well data were removed.

1A,B). Tissue culture-treated plates (TC plates) were well suited to discriminating between UTI89 and UTI89Δ*csgA*. Luminescence was detected with good sensitivity after both 24 and 48 h of growth in the white-bottom TC plates, with an acceptable Z' value, also known as the Z factor,[37] of 0.5 at 48 h (Figure 1A,B). Z' values of 0.5 or greater are predictive that valuable information can be obtained in a high-throughput screen. Data from the clear-bottom TC plates yielded poor Z' values when UTI89 and UTI89Δ*csgA* were compared at 24 h and resulted in a Z' value of 0.5 for the 48 h comparison. Assay plates with a "non-binding surface" (NBS) are also commercially available and were tested. Luminescence for both strains in NBS plates was very low at 24 h, and results at 48 h were inferior to the TC plates, with greater standard deviations and a poor Z' value (Figure S1). Thus, the white-bottom TC-treated plates and growth for 48 h were selected for the UTI89 curli-mediated biofilm HTS to ensure the maximum chance of success in identifying inhibitors that yield significant decreases in luminescence. The ability to quickly assess cell turbidity is not possible with white-bottom plates, but, as described below, was built into the parallel screen for curli-specific inhibitors by selecting clear-bottom plates in that assay.

Development of the Curli-Specific Adherence Inhibitor Screen. The screen described above would identify inhibitors that could be operating through a variety of mechanisms, including preventing the production of cellulose or curli or preventing their interactions or their postproduction ability to adhere to the plate well. Thus, we implemented a parallel screen to identify curli-specific inhibitors using the laboratory strain MC4100 most commonly used in curli biogenesis studies. MC4100 produces only curli fibers at the cell surface and does not produce other pili or cellulose. The adherence of MC4100 compared to MC4100Δ*csg* (MC4100 lacking the entire curli gene cluster) on each plate type was compared. The nonbinding surface plates performed extremely poorly with all luminescence values below 8500 and were not considered for the MC4100 HTS (Figure S1). The TC-treated plates were again optimal (Figure 1C,D). Accumulated biomass was detected at 24 h, and further accumulation was observed at 48 h (Figure 1C). Although the TC-treated white-bottom plates had a superior Z' value compared to the clear-bottom plates, an additional goal for this screen was to collect optical density data to roughly evaluate cell density. Thus, the clear-bottom TC plates with growth at 48 h were selected for MC4100. Additional analysis described below also improved the effective value of Z' in this assay. Finally, UT89 biofilm formation and MC4100 adhesion assays were performed with biomass detection using the fluorescent dye Hoechst 33342, which is a cell-permeable dye that quantifies the amount of DNA present in each well after washing, rather than the accessible ATP released from cells in the BacTiter-Glo assay. Although the Hoescht 33342 method is less desirable for a HTS due to background fluorescence, it provided an independent complementary assay and confirmed our expectations that the measured ATP levels using the BacTiter-Glo assay were associated with an increase in cell number (Figure S2).

Computational Analysis of Full-Plate Data. In preparation for high-throughput screening of the small NIH Clinical Collection (NIHCC) compound library as well as a much larger library, we ran tests with fully loaded 384-well plates with replicate control wells and sterile media wells. We observed that there was a gradient across the plate resulting in larger values of luminescence moving from columns 1 to 24, perhaps resulting from a thermal or aeration gradient. Edge wells around the plate exhibited higher signal, perhaps due to increased aeration or evaporative loss near the lid opening. We determined that this was not attributed to the kinetics of luminescence

DOI: 10.1021/acsinfecdis.5b00055
ACS Infect. Dis. 2015, 1, 460−468

generation and assay detection times (Figure S3). Bacterial growth-dependent assays, particularly this assay in the 384-well plate format with growth during 48 h, are susceptible to local environmental variations, and the effects were more noticeable in the MC4100 cell adherence assay than in the UTI89 biofilm assay. Thus, we removed edge-well data and additionally applied a plate-flattening algorithm (see Methods) to compare individual well values to the entire plate median rather than to a small subset of wells with control bacteria present at one location on the plate (Table 1). This provided an unbiased method to score plate wells and was used to determine effective Z' values for each assay. The Z' score for MC4100 adhesion by the BacTiter-Glo luminescence measurement improved from 0.35 to 0.64 considering these whole-plate data, and the Z' value for UTI89 improved slightly from 0.74 to 0.88 (Table 1). This analysis suggested that reliable hits could be obtained from high-throughput screening using these protocols. Without this comparative adjustment, the HTS may have been considered not valuable for MC4100 on the basis of the initial Z' value. Thus, the full control plate analysis was important to the final development and implementation of the HTS.

Table 1. Calculated Z' Values for Full-Plate Screening Tests with and without the Plate-Flattening Adjustment

	MC4100 absorbance	MC4100 luminescence	UTI89 luminescence
original data	0.51 ± 0.04	0.35 ± 0.03	0.74 ± 0.04
original data, flattened	0.64 ± 0.04	0.52 ± 0.04	0.84 ± 0.03
original data, edge wells removed	0.61 ± 0.04	0.47 ± 0.07	0.78 ± 0.05
edge wells removed, flattened	0.68 ± 0.04	0.64 ± 0.05	0.88 ± 0.02

Testing the NIHCC Compound Library. The NIHCC compound library of 446 small molecules was used to pilot our HTS. We applied the following initial selection criteria to identify strong "hits": (1) cell adherence for both UTI89 and MC4100 as reported by BacTiter-Glo must yield a luminescence reading of <50% of the untreated bacteria and (2) regarding cell viability, treated cells must yield an optical density value of >90% that of untreated cells (measured in the MC4100 assay with clear bottom plates). Using these criteria, one compound, rifapentine, was identified in each screen and was further characterized for its ability to prevent UTI89 biofilm formation and MC4100 curli-mediated adhesion. In the UTI89 biofilm assay, rifapentine-treated cells exhibited 47% of the relative luminescence of untreated cells; luminescence in the rifapentine-treated MC4100 assay was 22% that of untreated cells, with no difference in optical density compared to untreated cells.

Rifapentine is known as an antibiotic that inhibits bacterial RNA polymerase[38] and is present in the NIHCC compound library as it is used to treat tuberculosis. However, in our screen, rifapentine did not inhibit cell growth as revealed by the optical measurement, but inhibited biofilm formation. The NIHCC also contains other clinically available antibiotics, and these did exhibit typical antibiotic activity in our screen, as evidenced by reduced optical density data in the MC4100 assay. These data as well as the luminescence values from the UTI89 and MC4100 screens are provided in Table S1 and demonstrate the correlated reduction in viability and biofilm-associated BacTiter-Glo luminescence as cell growth was inhibited.

Rifapentine Inhibits Curli-Dependent Biofilm Formation on Plastic, on Agar, and at the Air−Liquid Interface. Additional curli-associated assays were performed to examine the influence of rifapentine on curli production and curli-associated phenotypes in MC4100 and UTI89. First, to directly follow up on the HTS screen, the inhibition of UTI89 biofilm formation and MC4100 adhesion on plastic was tested as a function of rifapentine concentration and was found to be effective at concentrations as low as 0.25 μM (Figure 2A) and did not affect the viability of cells at these concentrations (Figure 2B). During growth in nutrient broth, cells grow normally in concentrations up to 1.0 μM rifapentine (Figure 2B, left) but exhibit decreases in viability for concentrations >2 μM (Figure 2B, right). Resistance to rifapentine and other rifamycins is also possible through the emergence of one of several point mutations in *rpoB*.[39,40] The generation of spontaneous mutants was observed when *E. coli* MC4100 were grown at concentrations >5 μM in broth (Figure S4). Below this concentration, resistant mutants were not observed. The inhibition of curli-dependent adhesion and biofilm formation was observed at concentrations as low as 0.25 and 0.5 μM in broth, well below the concentration at which spontaneous mutants or growth defects were observed.

Growth and colony morphology were also observed for treated cells grown on agar. Visual inspection of the growth of a drop culture on agar after 24 and 48 h revealed that bacterial growth was not significantly reduced for rifapentine concentrations at or below 4 μM for MC4100 and 3 μM for UTI89 (Figure 2C). Also apparent from the agar photographs is the loss of the hallmark wrinkled morphology associated with UTI89, which requires the coproduction of curli and cellulose (Figure 2C). The concentrations of rifapentine required in the agar assay are higher than in the broth assays due to the depletion of compound from the underlying agar that decreases the effective concentration as a function of time. Electron micrographs revealed the marked inhibition of curli production at the cell surface of cells grown on rifapentine-supplemented agar (Figure 2D). Furthermore, rifapentine inhibited pellicle production (biofilm at the air−liquid interface) by UTI89 (Figure 2E). Thus, rifapentine inhibits curli-dependent biofilm formation on plastic, on agar, and at the air−liquid interface.

To examine whether the influence of rifapentine was compound-specific or class-specific, we also tested the influence of three other rifamycins (rifampin, rifaximine, and Rifamycin SV) in the colony growth and morphology assays. The ability to inhibit biofilm formation in a manner that is independent of cell killing, that is, at concentrations below which antibiotic activity dominates, is shared by the original compound, rifapentine, and rifampicin and rifaximine (Figure S5). Rifamycin SV did not reveal significant morphology changes until a concentration of 2−3 μM was supplemented in agar (Figure S5). Thus, the effects are not entirely class-specific, but are shared by three of the four tested compounds.

Rifapentine Inhibits Curli Production and Curli Gene Transcription. Because rifapentine was identified in both the UTI89 and MC4100 screens, we anticipated that its mode of action in inhibiting biofilm formation was either due to the inhibition of curli production or through preventing curli interactions with the substrate. We performed whole-cell Western blot analysis of cells grown on agar containing various concentrations of rifapentine to assess the potential influence of the compound on curli protein production. In the presence of increasing concentrations from 0.25 to 1.25 μM rifapentine in

DOI: 10.1021/acsinfecdis.5b00055
ACS Infect. Dis. 2015, 1, 460−468

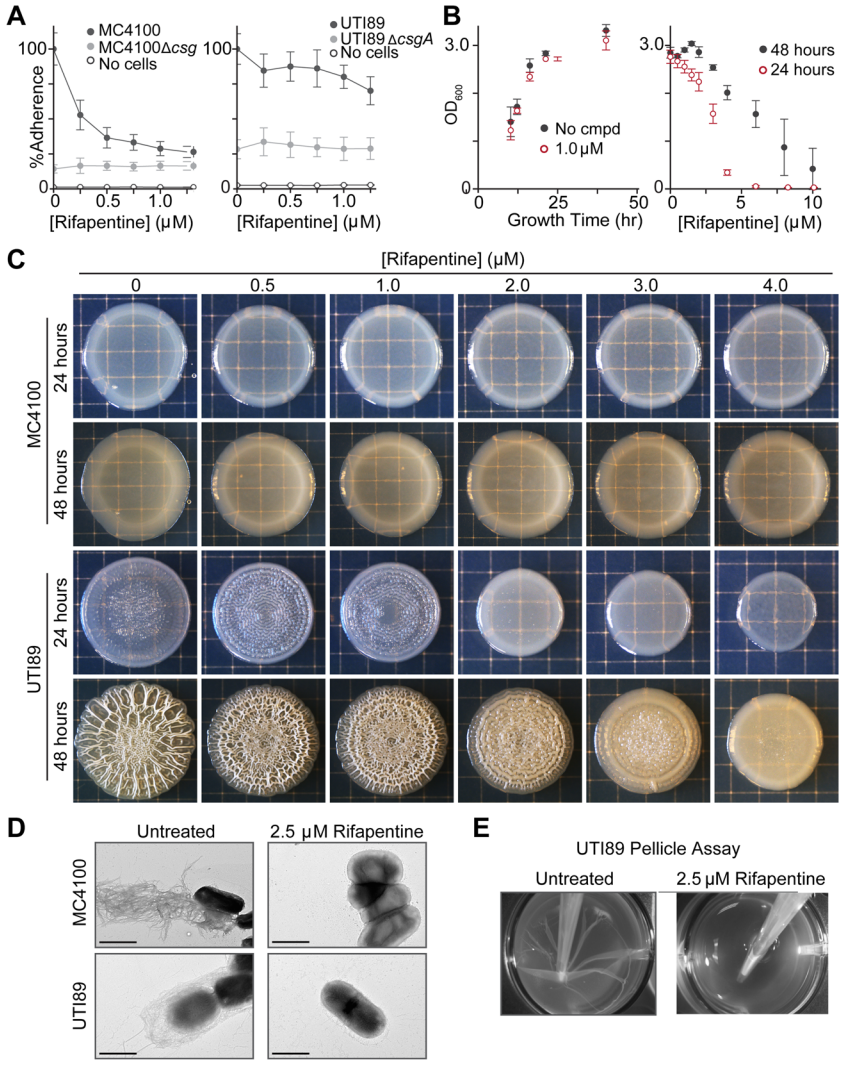

Figure 2. Rifapentine prevents curli production and curli-associated biofilm formation. (A) Rifapentine inhibits MC4100 and UTI89 biomass accumulation in the broth-based BacTiter Glo biofilm assay at concentrations as low as 0.25 μM in MC4100 and 1 μM in UTI89. (B) Rifapentine does not inhibit growth kinetics at 1 μM, but begins to affect growth at concentrations above 2.5 μM. Data are shown for MC4100. (C) Liquid drop culture growth of MC4100 and UTI89 on YESCA agar supplemented with various concentrations of rifapentine, observed after 24 and 48 h of growth. Loss of the curli-dependent wrinkled colony morphology is evident for rifapentine-treated UTI89. Small squares are 2 mm per side. (D) Transmission electron micrographs of cells grown on agar in the presence of 2.5 μM rifapentine reveal the loss of curli production. (E) Growth in the presence of rifapentine inhibits the hallmark wrinkled morphology associated with UTI89 biofilm formation. Rifapentine inhibits the formation of a pellicle, evaluated after 72 h of growth.

YESCA agar, cell-associated CsgA and CsgG levels decreased precipitously for MC4100 (Figure 3A). Inhibition of CsgA and CsgG was also observed for UTI89 and UTI89Δ*bcsA* at slightly higher concentrations (1−2 μM) of rifapentine (Figure 3A). UTI89Δ*bcsA* lacks the cellulose synthesis gene, *bcsA*, and was included in this assay because it produces curli but cannot form a biofilm due to the lack of cellulose. Thus, it is easier to resuspend and normalize by cell number (similar to MC4100) than UTI89. Results with all three strains were comparable. Cell-associated curli protein production was inhibited in MC4100, UTI89, and UTI89Δ*bcsA*. Ponceau S staining of these Western blot membranes confirmed that sample loading was even across all samples and demonstrated that total protein content in each sample was similar (Figure S6), whereas the Western blot was able to detect the specific reduction in cell-associated CsgA and CsgG in the presence of increasing concentrations of rifapentine.

Quantitative real-time PCR of cells grown in the same way revealed that the amount of mRNA from each of the curli genes (*csgA*, *csgB*, *csgD*, *csgE*, *csgF*, and *csgG*) was decreased in response to rifapentine after 24 h (Figure 3B) and 48 h (Figure S7) of growth. CsgD is the major regulator of curli synthesis, driving transcription of the *csgDEFG* and the *csgBA* operons, so it is expected for transcription of all curli genes to be down-regulated when *csgD* transcription is inhibited. The levels of *csgB* were always the most dramatically reduced, as measured in three separate sample preparations. Expression of *rpoS*, a major subunit of RNA polymerase, was not significantly affected. RpoS is the master regulator of the general stress response and of stationary phase gene expression in *E. coli*. Thus, rifapentine is not exerting a general stress or influencing global regulation of stationary phase gene expression and appears to be operating further down the cascade in the regulation of curli gene expression. The expressions of the cellulose-related genes *bcsA* and *adrA* were also decreased at 24 h (Figure 3B) and 48 h

DOI: 10.1021/acsinfecdis.5b00055
ACS Infect. Dis. 2015, 1, 460−468

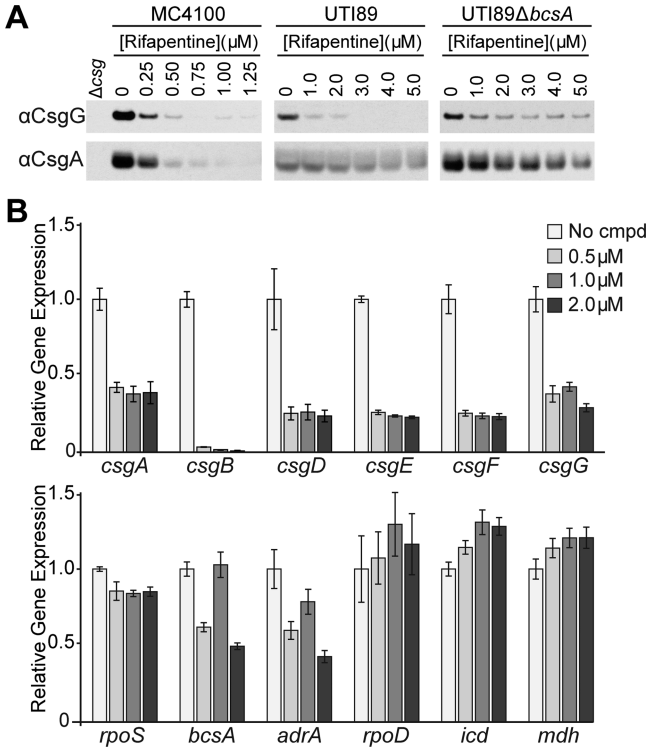

Figure 3. Quantitative profiling of curli protein production and gene transcription. (A) Whole-cell Western blot profiling of CsgA and CsgG levels of MC4100, UTI89, and UTI89Δ*bcsA* grown on YESCA nutrient agar for 48 h as a function of the supplemented rifapentine concentration demonstrate that CsgA levels are decreased in the presence of rifapentine. Reductions in cell-associated protein levels are observed at concentrations as low as 0.25 μM in MC4100 and 1 μM in UTI89 and UTI89Δ*bcsA*. (B) qRT-PCR performed on MC4100 grown for 24 h reveals that mRNA for each curli protein is reduced when grown in the presence of rifapentine. Results for 48 h samples are similar (Figure S7). All samples (A, B) contained 0.1% vol/vol DMSO.

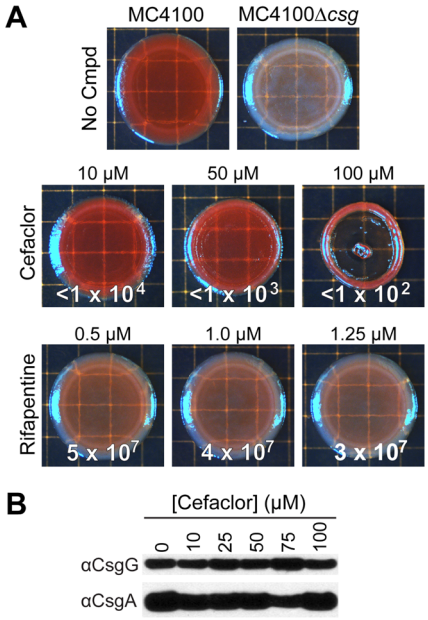

Figure 4. Cefaclor does not decrease curli production. (A) Congo red binding attributed to curli production in MC4100 is not affected by Cefaclor. CR binding is inhibited at Rifapentine concentrations of 0.5 μM and higher, whereas Cefaclor does not inhibit CR binding, even as cell viability is severely impaired. (B) CsgA and CsgG levels on a per cell basis in MC4100 are not affected by Cefaclor, as determined by whole-cell Western blot analysis.

(Figure S7). These are also influenced by the CsgD transcription factor, encoded for by *csgD*, which was inhibited. Many small RNAs produced in response to environmental changes can inhibit the *csgD*-driven transcription factor cascade and can be considered in future work. Expression of the housekeeping genes *rpoD* (sigma-70), *icd* (isocitrate dehydrogenase), and *mdh* (malate dehydrogenase) was not affected by rifapentine treatment.

General Antibiotic Treatment Does Not Inhibit Curli Production. Finally, we sought to determine how curli production might be influenced by conventional antibiotic pressure. Congo red binding phenotypes suggested that although Cefaclor was reducing cell growth on agar, curli were still being produced by MC4100 as the bacteria took up the amyloid dye, Congo red (Figure 4A). Rifapentine, however, reduced Congo red uptake at a concentration as low as 0.5 mM, before growth defects are observed, consistent with the reduction in curli production. Growth in 100 μM Cefaclor is severely impaired, but even where some growth occurs at the edges of the culture drop, the bacteria take up Congo red (Figure 4A). Corresponding viability data for MC4100 grown in the presence of the indicated concentrations of compound are provided at the bottom of each photograph. Western blots of Cefaclor-treated cells demonstrated definitively that even though cell viability was decreasing due to Cefaclor treatment, curli production per cell was not altered (Figure 4B). Thus, general antibiotic pressure does not itself inhibit curli production, and the action of rifapentine in inhibiting curli gene transcription is independent of killing cells.

Collectively, our results describe the unanticipated influence of rifapentine in the prevention of bacterial biofilm formation by uropathogenic *E. coli*. Our optimized HTS and analysis protocol allows one to identify potent *E. coli* adhesion and biofilm inhibitors (and, simultaneously, to potentially identify compounds that target cell viability) by taking into account the variations in cell growth and biofilm formation that can occur in 384-well plates. Additional compounds are being identified through the screening results of larger libraries. Furthermore, inhibitors that interrupt curli fiber assembly or prevent biofilm formation through physical interactions with curli or biofilm matrix parts, rather than through the inhibition of gene transcription, may also be of therapeutic value and can additionally be used in chemical genetics approaches to help probe assembly processes.

METHODS

Bacterial Strains and Growth Conditions. The UPEC strain UTI89 and the curli mutant UTI89Δ*csgA* were used for curli-mediated biofilm formation assays. The laboratory strain MC4100 and the curli mutants MC4100Δ*csgA*, MC4100Δ*csgB*, and MC4100Δ*csg* were used for the curli-only adhesion screening. All bacteria were grown in YESCA (1 g/L yeast extract, 10 g/L casamino acids) nutrient broth at 26 °C. For 384-well plate assays, cells from an overnight culture were used to inoculate media in a 1:300 ratio, and 50 μL of inoculated media was added to each well.

Selection of 384-Well Plate Type. The following plate types were tested in the biofilm and curli adhesion assays: untreated white (Corning no. 3572), NBS white with clear

DOI: 10.1021/acsinfecdis.5b00055
ACS Infect. Dis. 2015, 1, 460−468

bottom (Corning no. 3653), TC-treated white (Corning no. 3570), and TC-treated white with clear bottom (Corning no. 3707) plates.

BacTiter-Glo Cell Adherence Assay. After growth, the optical density at 600 nm was measured. Plates were washed with 70 μL of 1× PBS per well for five cycles on a Bio-Tek plate washer (ELx405CW) to remove planktonic cells. For detection of adherent cells using BacTiter-Glo (Promega no. G8232), the BacTiter-Glo reagent was diluted in sterile YESCA broth at a ratio of 1:10, and 70 μL was added to each well. The plates were incubated without shaking at room temperature for approximately 15−30 min before the luminescence was read. Optical density and luminescence were read on a Tecan infinite M1000 plate reader.

Hoechst 33342 Cell Adherence Assay. A solution of 1 μg/mL Hoechst 33342 and 1 mg/mL lysozyme was prepared in TE buffer (10 mM Tris, 1 mM EDTA, pH 8.0). For detection of adherent cells, plates were washed as described above, then filled with 70 μL/well of the Hoechst 33342 solution. Plates were incubated in the dark for approximately 1 h, and fluorescence was measured (λ_{ex}, 350 nm; λ_{em}, 461 nm).

384-Well Plate NIHCC Assay. Plates were set up as above, except for the following changes. Each plate was filled with 40 μL per well of sterile YESCA, to which the 446 NIH Clinical Collection (NIHCC) library compounds were added using the Sciclone ALH3000. Overnight starter cultures were used to inoculate YESCA broth at a 1:60 ratio, and 10 μL of this inoculated media was added to each well. Cells were grown for 48 h and then analyzed with BacTiter-Glo.

Computational Analysis of Full-Plate Data. To examine the 384-well plate assay under full-plate testing conditions, columns 1 and 2 were designated control cell wells containing bacteria in YESCA broth and no compounds. Columns 3 through 22 were identical to columns 1 and 2, although in the planned screen, these would contain test compounds. Columns 23 and 24 contained only sterile media. All wells in columns 1 and 22 and rows A and P were considered "edge wells" for data processing. Because a gradient was observed across the plate, rather than having identical values for columns 1−22, a plate-flattening algorithm was implemented to permit better comparison of data and identification of true hits. This simply involved determining the plate median, which was calculated as the median of all test wells, excluding edge wells. Each row was then normalized to the plate median. In each row, the individual well values were adjusted to make the row median equal to the plate median, and each column was adjusted similarly. All well values were then normalized to the plate median.

Western Blot Assay. Cell-associated curli proteins CsgA and CsgG were examined by immunoblot assays. To inoculate colonies, 10 μL of overnight cultures of MC4100, MC4100Δ*csg*, UTI89, and UTI89Δ*bcsA* was spotted on YESCA agar containing various concentrations of rifapentine (with final DMSO concentration of 0.1% in each sample) for 48 h. For MC4100, MC4100Δ*csg*, and UTI89Δ*bcsA* samples, harvested cells were resuspended in PBS, and normalized whole-cell samples with equivalent cell numbers were prepared as cell pellets of 1 mL of cell suspension in 1× PBS with an optical density at 600 nm (OD600) of 1.0. For UTI89 samples, the entire colony was washed with PBS and pelleted without normalization due to the difficulty of dispersing the cells in the biofilm. Each pellet was treated with 200 μL (500 μL for UTI89 samples) of >88% formic acid to dissociate CsgA subunits. Formic acid was removed by vacuum centrifugation, and samples were resuspended in 500 μL (1000 μL for UTI89 samples) of sodium dodecyl sulfate−polyacrylamide gel electrophoresis (SDS-PAGE) loading buffer. Protein gel electrophoresis was carried out using 12% SDS-PAGE gels (Invitrogen) and blotted onto 0.2 μm pore size nitrocellulose transfer membranes (Whatman). After transfer, membranes were stained with Ponceau S (Amresco no. K793) for visualization of total protein levels. The polyclonal rabbit antiserum to CsgA or CsgG was used as the primary antibody, and horseradish peroxidase (HRP)-conjugated goat anti-rabbit antibody (Pierce) was used as the secondary antibody.

Quantitative Real-Time PCR Assay. Expression of curli proteins was examined by qRT-PCR. To inoculate colonies, four 15 μL aliquots of overnight cultures of MC4100 were spotted on each YESCA agar plate containing various concentrations of rifapentine (with final DMSO concentration of 0.1% in each sample) and grown for 24 h. The RNA was stabilized using RNAprotect Bacteria Reagent (Qiagen no. 76506) and then isolated using the RNeasy Mini Kit (Qiagen no. 74104). Synthesis of cDNA was carried out using the High-Capacity cDNA Reverse Transcription Kit (Applied Biosystems no. 4368813). The real-time PCR measurements were performed on the Applied Biosystems StepOne Plus system using Power SYBR Green PCR Master Mix (Applied Biosystems no. 4367659). The $\Delta\Delta C_T$ method[38] was used for analysis of the qRT-PCR data, using MC4100 grown without rifapentine as the reference sample. All cDNA levels were normalized to levels of *rrsH* (16S rRNA) from the same sample. Primers used are listed in Table S2.

Transmission Electron Microscopy. UTI89 and MC4100 were grown on YESCA agar with or without 2.5 μM rifapentine for 48 h at 26 °C. Bacteria cells were harvested from agar plates and resuspended in 1× PBS. The harvested cell suspension was applied directly onto 300-mesh copper grids coated with Formvar film (Electron Microscopy Sciences, Hatfield, PA, USA) for 2 min. The samples in grids were washed five times with deionized water and negatively stained with 2% uranyl acetate for 90 s. After 5 min of drying, the TEM samples were examined with a JEOL 1400 electron microscope (JEOL USA, Peabody, MA, USA).

Agar Biofilm Morphology Assay. Biofilm formation on agar plates was initiated by spotting 10 μL of an overnight starter culture of UTI89 onto each YESCA agar plate with or without rifapentine (final concentration, 2.5 μM). The associated biofilm morphology was observed after 48 h of growth at 26 °C.

Pellicle Assay. Pellicle formation was initiated by inoculating 2 μL of an overnight starter culture of UTI89 in 2 mL of YESCA broth in 24-well plate wells containing various concentrations of rifapentine and incubated at 26 °C. Pellicle formation was inspected visually and assessed by perturbation with a pipet tip after 48 h of growth.

■ ASSOCIATED CONTENT

Supporting Information

The Supporting Information is available free of charge on the ACS Publications website at DOI: 10.1021/acsinfecdis.5b00055.

Figures S1−S7 and Tables S1 and S2 (PDF)

DOI: 10.1021/acsinfecdis.5b00055
ACS Infect. Dis. 2015, 1, 460−468

AUTHOR INFORMATION

Corresponding Author

*(L.C.) E-mail: cegelski@stanford.edu. Phone: (650) 725-3527. Fax: (650) 723-4817.

Notes

The authors declare no competing financial interest.

ACKNOWLEDGMENTS

We gratefully acknowledge support from the NIH Director's New Innovator Award (DP20D007488 to L.C.) and the Abbott Laboratories Stanford Graduate Fellowship (M.C.M.). We thank Dr. David E. Solow-Cordero and Jason Wu from the Stanford High-Throughput Bioscience Center (HTBC) and NCRR NIH Instrumentation grant numbers S10RR019513 and S10RR026338. We thank Professor Matthew Chapman for providing the strain UTI89Δ*bcsA*.

REFERENCES

(1) Hall-Stoodley, L., Costerton, J. W., and Stoodley, P. (2004) Bacterial biofilms: from the natural environment to infectious diseases. *Nat. Rev. Microbiol. 2*, 95−108.

(2) Donlan, R. M., and Costerton, J. W. (2002) Biofilms: survival mechanisms of clinically relevant microorganisms. *Clin. Microbiol. Rev. 15*, 167−193.

(3) Costerton, J. W., Stewart, P. S., and Greenberg, E. P. (1999) Bacterial biofilms: a common cause of persistent infections. *Science 284*, 1318−1322.

(4) Watnick, P., and Kolter, R. (2000) Biofilm, city of microbes. *J. Bacteriol. 182*, 2675−2679.

(5) Cegelski, L., Marshall, G. R., Eldridge, G. R., and Hultgren, S. J. (2008) The biology and future prospects of antivirulence therapies. *Nat. Rev. Microbiol. 6*, 17−27.

(6) Romling, U., Kjelleberg, S., Normark, S., Nyman, L., Uhlin, B. E., and Akerlund, B. (2014) Microbial biofilm formation: a need to act. *J. Intern. Med. 276*, 98−110.

(7) Cegelski, L., Marshall, G. R., Eldridge, G. R., and Hultgren, S. J. (2008) The biology and future prospects of antivirulence therapies. *Nat. Rev. Microbiol. 6*, 17−27.

(8) Watnick, P., and Kolter, R. (2000) Biofilm, city of microbes. *J. Bacteriol. 182*, 2675−2679.

(9) Mulvey, M. A. (2002) Adhesion and entry of uropathogenic *Escherichia coli*. *Cell. Microbiol. 4*, 257−271.

(10) Connell, I., Agace, W., Klemm, P., Schembri, M., Mărild, S., and Svanborg, C. (1996) Type 1 fimbrial expression enhances *Escherichia coli* virulence for the urinary tract. *Proc. Natl. Acad. Sci. U. S. A. 93*, 9827−9832.

(11) Mulvey, M. A., Lopez-Boado, Y. S., Wilson, C. L., Roth, R., Parks, W. C., Heuser, J., and Hultgren, S. J. (1998) Induction and evasion of host defenses by type 1-piliated uropathogenic *Escherichia coli*. *Science 282*, 1494−1497.

(12) Kai-Larsen, Y., Luthje, P., Chromek, M., Peters, V., Wang, X., Holm, A., Kadas, L., Hedlund, K. O., Johansson, J., Chapman, M. R., Jacobson, S. H., Romling, U., Agerberth, B., and Brauner, A. (2010) Uropathogenic *Escherichia coli* modulates immune responses and its curli fimbriae interact with the antimicrobial peptide LL-37. *PLoS Pathog. 6*, e1001010.

(13) Cegelski, L., Pinkner, J. S., Hammer, N. D., Cusumano, C. K., Hung, C. S., Chorell, E., Aberg, V., Walker, J. N., Seed, P. C., Almqvist, F., Chapman, M. R., and Hultgren, S. J. (2009) Small-molecule inhibitors target *Escherichia coli* amyloid biogenesis and biofilm formation. *Nat. Chem. Biol. 5*, 913−919.

(14) Bian, Z., Brauner, A., Li, Y., and Normark, S. (2000) Expression of and cytokine activation by *Escherichia coli* curli fibers in human sepsis. *J. Infect. Dis. 181*, 602−612.

(15) Tukel, C., Nishimori, J. H., Wilson, R. P., Winter, M. G., Keestra, A. M., van Putten, J. P., and Baumler, A. J. (2010) Toll-like receptors 1 and 2 cooperatively mediate immune responses to curli, a common amyloid from enterobacterial biofilms. *Cell. Microbiol. 12*, 1495−1505.

(16) Rapsinski, G. J., Newman, T. N., Oppong, G. O., van Putten, J. P., and Tükel, C. (2013) CD14 protein acts as an adaptor molecule for the immune recognition of *Salmonella* curli fibers. *J. Biol. Chem. 288*, 14178−14188.

(17) Rapsinski, G. J., Newman, T. N., Oppong, G. O., van Putten, J. P., and Tükel, C. (2013) CD14 protein acts as an adaptor molecule for the immune recognition of *Salmonella* curli fibers. *J. Biol. Chem. 288*, 14178−14188.

(18) Boyer, R. R., Sumner, S. S., Williams, R. C., Pierson, M. D., Popham, D. L., and Kniel, K. E. (2007) Influence of curli expression by *Escherichia coli* 0157:H7 on the cell's overall hydrophobicity, charge, and ability to attach to lettuce. *J. Food Prot. 70*, 1339−1345.

(19) Ryu, J. H., Kim, H., and Beuchat, L. R. (2004) Attachment and biofilm formation by *Escherichia coli* O157:H7 on stainless steel as influenced by exopolysaccharide production, nutrient availability, and temperature. *J. Food Prot. 67*, 2123−2131.

(20) Barak, J. D., Gorski, L., Naraghi-Arani, P., and Charkowski, A. O. (2005) *Salmonella enterica* virulence genes are required for bacterial attachment to plant tissue. *Appl. Environ. Microbiol. 71*, 5685−5691.

(21) Barnhart, M. M., and Chapman, M. R. (2006) Curli biogenesis and function. *Annu. Rev. Microbiol. 60*, 131−147.

(22) Pawar, D. M., Rossman, M. L., and Chen, J. (2005) Role of curli fimbriae in mediating the cells of enterohaemorrhagic *Escherichia coli* to attach to abiotic surfaces. *J. Appl. Microbiol. 99*, 418−425.

(23) Vidal, O., Longin, R., Prigent-Combaret, C., Dorel, C., Hooreman, M., and Lejeune, P. (1998) Isolation of an *Escherichia coli* K-12 mutant strain able to form biofilms on inert surfaces: involvement of a new ompR allele that increases curli expression. *J. Bacteriol. 180*, 2442−2449.

(24) Uhlich, G. A., Gunther, N. W. t., Bayles, D. O., and Mosier, D. A. (2009) The CsgA and Lpp proteins of an *Escherichia coli* O157:H7 strain affect HEp-2 cell invasion, motility, and biofilm formation. *Infect. Immun. 77*, 1543−1552.

(25) Lim, J. Y., May, J. M., and Cegelski, L. (2012) Dimethyl sulfoxide and ethanol elicit increased amyloid biogenesis and amyloid-integrated biofilm formation in *Escherichia coli*. *Appl. Environ. Microbiol. 78*, 3369−3378.

(26) Saldana, Z., Xicohtencatl-Cortes, J., Avelino, F., Phillips, A. D., Kaper, J. B., Puente, J. L., and Giron, J. A. (2009) Synergistic role of curli and cellulose in cell adherence and biofilm formation of attaching and effacing *Escherichia coli* and identification of Fis as a negative regulator of curli. *Environ. Microbiol. 11*, 992−1006.

(27) Gualdi, L., Tagliabue, L., Bertagnoli, S., Ierano, T., De Castro, C., and Landini, P. (2008) Cellulose modulates biofilm formation by counteracting curli-mediated colonization of solid surfaces in *Escherichia coli*. *Microbiology 154*, 2017−2024.

(28) Chapman, M. R., Robinson, L. S., Pinkner, J. S., Roth, R., Heuser, J., Hammar, M., Normark, S., and Hultgren, S. J. (2002) Role of *Escherichia coli* curli operons in directing amyloid fiber formation. *Science 295*, 851−855.

(29) Robinson, L. S., Ashman, E. M., Hultgren, S. J., and Chapman, M. R. (2006) Secretion of curli fibre subunits is mediated by the outer membrane-localized CsgG protein. *Mol. Microbiol. 59*, 870−881.

(30) Hammar, M., Bian, Z., and Normark, S. (1996) Nucleator-dependent intercellular assembly of adhesive curli organelles in *Escherichia coli*. *Proc. Natl. Acad. Sci. U. S. A. 93*, 6562−6566.

(31) Nenninger, A. A., Robinson, L. S., and Hultgren, S. J. (2009) Localized and efficient curli nucleation requires the chaperone-like amyloid assembly protein CsgF. *Proc. Natl. Acad. Sci. U. S. A. 106*, 900−905.

(32) Cegelski, L., Pinkner, J. S., Hammer, N. D., Cusumano, C. K., Hung, C. S., Chorell, E., Aberg, V., Walker, J. N., Seed, P. C., Almqvist, F., Chapman, M. R., and Hultgren, S. J. (2009) Small-molecule inhibitors target *Escherichia coli* amyloid biogenesis and biofilm formation. *Nat. Chem. Biol. 5*, 913−919.

DOI: 10.1021/acsinfecdis.5b00055
ACS Infect. Dis. 2015, 1, 460−468

(33) Peters, J. E., Thate, T. E., and Craig, N. L. (2003) Definition of the *Escherichia coli* MC4100 genome by use of a DNA Array. *J. Bacteriol. 185*, 2017−2021.
(34) Hadjifrangiskou, M., Gu, A. P., Pinkner, J. S., Kostakioti, M., Zhang, E. W., Greene, S. E., and Hultgren, S. J. (2012) Transposon mutagenesis identifies uropathogenic *Escherichia coli* biofilm factors. *J. Bacteriol. 194*, 6195−6205.
(35) O'Toole, G. A., and Kolter, R. (1998) Initiation of biofilm formation in *Pseudomonas fluorescens* WCS365 proceeds via multiple, convergent signalling pathways: a genetic analysis. *Mol. Microbiol. 28*, 449−461.
(36) Junker, L. M., and Clardy, J. (2007) High-throughput screens for small-molecule inhibitors of *Pseudomonas aeruginosa* biofilm development. *Antimicrob. Agents Chemother. 51*, 3582−3590.
(37) Zhang, J.-H., Chung, T. D. Y., and Oldenburg, K. R. (1999) A simple statistical parameter for use in evaluation and validation of high throughput screening assays. *J. Biomol. Screening 4*, 67−73.
(38) Pfaffl, M. W. (2001) A new mathematical model for relative quantification in real-time RT-PCR. *Nucleic Acids Res. 29*, 45e.
(39) Moghazeh, S. L., Pan, X., Arain, T., Stover, C. K., Musser, J. M., and Kreiswirth, B. N. (1996) Comparative antimycobacterial activities of rifampin, rifapentine, and KRM-1648 against a collection of rifampin-resistant *Mycobacterium tuberculosis* isolates with known rpoB mutations. *Antimicrob. Agents Chemother. 40*, 2655−2657.
(40) Williams, D. L., Spring, L., Collins, L., Miller, L. P., Heifets, L. B., Gangadharam, P. R. J., and Gillis, T. P. (1998) Contribution of rpoB mutations to development of rifamycin cross-resistance in *Mycobacterium tuberculosis*. *Antimicrob. Agents Chemother. 42*, 1853−1857.

■ NOTE ADDED AFTER ASAP PUBLICATION

This paper was published ASAP on August 11, 2015, with an error in the Abstract. The corrected version was reposted on September 8, 2015.

DOI: 10.1021/acsinfecdis.5b00055
ACS Infect. Dis. 2015, 1, 460−468